Title

Neuromyelitis optica IgG does not alter aquaporin-4 water permeability, plasma membrane M1/M23 isoform content, or supramolecular assembly

Journal

Glia, 60(12)

ISSN

0894-1491

Authors

Rossi, Andrea
Ratelade, Julien
Papadopoulos, Marios C
et al.

Publication Date

2012-12-01

DOI

10.1002/glia.22417

Peer reviewed

Published in final edited form as:
Glia. 2012 December ; 60(12): 2027–2039. doi:10.1002/glia.22417.

Neuromyelitis Optica IgG Does Not Alter Aquaporin-4 Water Permeability, Plasma Membrane M1/M23 Isoform Content, or Supramolecular Assembly

Andrea Rossi[1,2], **Julien Ratelade**[1,2], **Marios C. Papadopoulos**[3], **Jeffrey L. Bennett**[4,5], and **A. S. Verkman**[1,2,*]

[1]Department of Medicine, University of California, San Francisco, California

[2]Department of Physiology, University of California, San Francisco, California

[3]Academic Neurosurgery Unit, St. George's, University of London, London, United Kingdom

[4]Department of Neurology, University of Colorado Denver, Aurora, Colorado

[5]Department of Ophthalmology, University of Colorado Denver, Aurora, Colorado

Abstract

Neuromyelitis optica (NMO) is thought to be caused by immunoglobulin G autoantibodies (NMO-IgG) against astrocyte water channel aquaporin-4 (AQP4). A recent study (Hinson et al. (2012) Proc Natl Acad Sci USA 109:1245- 1250) reported that NMO-IgG inhibits AQP4 water permeability directly and causes rapid cellular internalization of the M1 but not M23 isoform of AQP4, resulting in AQP4 clustering, enhanced complement-dependent cytotoxicity, and tissue swelling. Here, we report evidence challenging this proposed mechanism of NMO-IgG-mediated pathology. We measured osmotic water permeability by stopped-flow light scattering on plasma membrane vesicles isolated from AQP4-expressing CHO cells, an approach that can detect changes in water permeability as small as 5% and is not confounded by internalization effects. We found similar single- molecule water permeability for M1-AQP4 tetramers and M23-AQP4 clusters (orthogonal arrays of particles, OAPs). Exposure of AQP4 to high concentrations of NMOIgG from six seropositive NMO patients, and to high-affinity recombinant monoclonal NMO antibodies, did not reduce AQP4 water permeability. Also, NMO-IgG did not reduce water permeability in AQP4-reconstituted proteoliposomes. In transfected cells expressing M1- or M23-AQP4 individually, NMO-IgG caused more rapid internalization of M23- than M1-AQP4. In cells coexpressing both isoforms, M1- and M23-AQP4 comingled in OAPs that were internalized together in response to NMO-IgG. Super-resolution imaging and native gel electrophoresis showed that the size of AQP4 OAPs was not altered by NMO sera or recombinant NMO antibodies. We conclude that NMO-IgG does not: (i) inhibit AQP4 water permeability, (ii) cause preferential internalization of M1-AQP4, or (iii) cause intramembrane AQP4 clustering.

Keywords

AQP4; aquaporin; OAP; NMO; astrocyte

*Correspondence to: Alan S. Verkman, MD, PhD, 1246 Health Sciences East Tower, University of California, San Francisco, CA 94143-0521, USA. alan.verkman@ucsf.edu.

Additional Supporting Information may be found in the online version of this article.

INTRODUCTION

Neuromyelitis optica (NMO) is a demyelinating disease of the central nervous system (CNS) with inflammatory lesions seen mainly in spinal cord and optic nerve (Jarius and Wildemann, 2010; Papadopoulos and Verkman, 2012). Most NMO patients have in their serum immunoglobulin G (IgG) autoantibodies against aquaporin-4 (AQP4) (Lennon et al., 2005), a water channel expressed at the plasma membrane (PM) of astrocyte end-feet (Nielsen et al., 1997; Rash et al., 1998). Evidence from rodent models (Bennett et al., 2009; Bradl et al., 2009; Kinoshita et al., 2009; Saadoun et al., 2010) and clinical data (Jarius and Wildemann, 2010; Misu et al., 2007; Roemer et al., 2007; Wingerchuk et al., 2006) suggests that the autoantibody, called NMO-IgG (or AQP4-IgG), is pathogenic in NMO. Although the precise mechanism linking NMO-IgG to NMO pathology remains unclear, NMO-IgG binding to AQP4 on astrocytes is believed to recruit and activate complement, leading to membrane attack complex formation and primary astrocyte injury (complement-dependent cytotoxicity, CDC). This primary process induces leukocyte infiltration and cytokine release, which secondarily damages oligodendrocytes and neurons (Jarius and Wildemann, 2010; Papadopoulos and Verkman, 2012).

AQP4 is expressed as long (M1) and short (M23) isoforms, the latter forming supramolecular aggregates called orthogonal arrays of particles (OAPs) (Verbavatz et al., 1997; Yang et al., 1996). We demonstrated that AQP4 assembly in OAPs greatly enhances NMO-IgG-dependent CDC by two distinct mechanisms: increased affinity of NMO-IgG binding to OAPs vs. AQP4 tetramers (Crane et al., 2011) and multivalent interaction of complement protein C1q with clustered NMO-IgG on AQP4 OAPs (Phuan et al., 2012).Hinson et al. (2012) recently reported that M1-AQP4 is rapidly internalized following NMO-IgG binding, whereas M23-AQP4 resists internalization, and that NMO-IgG inhibits AQP4 water permeability. On the basis of these findings, they proposed a new mechanism of NMO pathogenesis in which NMO-IgG-induced internalization of M1-AQP4 and direct inhibition of AQP4 water permeability result in increased OAP size, enhanced CDC, and local tissue swelling. If correct, this mechanism has important implications regarding the initiating events in NMO pathogenesis and new treatment strategies.

Although the mechanism proposed by Hinson et al. (2012) is interesting, their major findings were quite unexpected based on the known biology of AQP4 and appear to conflict with the published literature. The differential internalization of M1-AQP4 and M23-AQP4 following NMO-IgG exposure is surprising, as M1- and M23-AQP4 form tight heterotetramers in cell PMs (Neely et al., 1999; Rossi et al., 2012a; Tajima et al., 2010). Differential internalization of M1- and M23-AQP4 conflicts with an earlier report by Hinson et al. (2008) showing full internalization of AQP4 and data from our laboratory showing rapid internalization of M1- and M23-AQP4 in transfected cells (Phuan et al., 2012). One technical concern with the Hinson et al. (2012) study was the use of N-terminus green fluorescent protein (GFP)-labeled AQP4, as the GFP label prevents OAP formation (Pisani et al., 2011; Rossi et al. 2012a; Tajima et al., 2010). It is also unlikely that significant inhibition of water permeability by NMO-IgG is sterically possible because of the large size of NMO-IgG compared with AQP4 tetramers, which consist of four monomers each containing separate water pores (Ho et al., 2009). Two laboratories have reported, using different methods, that NMO-IgG does not inhibit AQP4 water permeability (Melamud et al., 2012; Nicchia et al., 2009). Last, there appears to be a conceptual concern in the Hinson et al. (2012) study where it was argued that punctate AQP4, cell edema, and intramyelinic edema can occur in human NMO when NMO-IgG binds AQP4 without complement. This contradicts data in mouse models, where such changes occur only when complement is present (Saadoun et al., 2010), and histopathologic findings in human NMO showing marked astrocyte loss and deposition of activated complement in early NMO lesions (Parratt

and Prineas, 2010). Punctate AQP4 is a general, nonspecific finding seen in damaged astrocytes and myocytes (Anders and Brightman, 1982), as is cellular and intramyelinic edema, which are seen in other CNS diseases, such as Alexander disease, where NMO-IgG is absent (Brenner et al., 2001).

Here, we reexamined the key conclusions of Hinson et al. (2012) using quantitative biophysical methods that are not subject to technical artifact or sampling bias. Using multiple NMO patient sera and purified recombinant NMO antibodies, we found that NMO-IgG neither inhibits AQP4 water permeability nor causes preferential cellular internalization of M1-AQP4 or OAP clustering. Some of the data reported here are mentioned in a letter-to-the-editor (Rossi et al., 2012b) challenging the Hinson et al. (2012) study.

MATERIALS AND METHODS

DNA Constructs

cDNAs encoding human M1- and M23-AQP4 were PCR-amplified using whole-brain cDNA as template. PCR fragments were ligated into mammalian expression vector pcDNA3.1. To generate AQP4 C-terminal or N-terminal chimeras with fluorescent proteins, the respective sequences were PCR-amplified and ligated inframe into pEGFP-N1, pEGFP-C1, pmCherry-N1, and photoactivatable mCherry (PAmCherry)-N1 (Clontech, Mountain View, CA). M1- and M23-AQP4 fragments were also ligated in a bidirectional vector (PbI) (Clontech). All constructs were verified by sequencing.

Cell Culture and Transfections

U87MG (human glioblastoma-astrocytoma, ATCC HTB-14) and CHO-K1 (ATCC CCL-61) cells were maintained at 37°C in 5% CO_2, 95% air in appropriate medium (without phenol red) containing 10% FBS, 100 U/mL penicillin, and 100 μg/mL streptomycin, as described (Crane et al., 2011). Cells were transfected with cDNAs in antibiotic-free medium 12–24 h before experiments using TransIT-LT1 (Mirus, Madison, WI) at a 3:1 ratio (μL:μg nucleic acid) and 0.18 μg DNA/cm^2. Stable AQP4-expressing clones were selected following enrichment in Geneticin (Invitrogen, Carlsbad, CA) and plating in 96-well plates at low density.

NMO Sera and Recombinant Monoclonal Antibodies

Purified human monoclonal recombinant NMO-IgGs (rAb)-53 and rAb-58 were generated as described (Bennett et al., 2009), with a measles virus-specific rAb (2B4) used as an isotype-matched control. Labeling of rAb-58 with the red fluorophore Cy3 (rAb-58-Cy3) was done using the Amersham Cy3 Ab Labelling Kit (GE Health-care, Buckinghamshire, UK). NMO serum from six seropositive NMO patients was provided by Accelerated Cure (Waltham, MA). Control (non-NMO) human serum was obtained from three non-NMO individuals. For some studies, total IgG was purified and concentrated from serum using a Melon Gel IgG Purification Kit (Thermo Fisher Scientific, Rockford, IL) and Amicon Ultra Centrifugal Filter Units (Millipore, Billerica, MA). A point mutation was introduced into the IgG1 Fc sequence of the rAb-53 heavy chain to produce an “aquaporumab" (AQmab) that selectively lacks CDC effector function, as described (Tradtrantip et al., 2012).

Subcellular Fractionation

CHO cells stably expressing M1- or M23-AQP4 were homogenized in homogenizing buffer [300 mM sucrose, 1 mM EDTA, protease cocktail inhibitor (Roche, Basel, Switzerland), and 10 mM Tris–HCl (pH 7.2)] by a glass Dounce homogenizer. The homogenate was centrifuged at 500*g* for 10 min at 4°C and adjusted to 1.4 M sucrose, 10 mM Tris–HCl, and 0.2 mM EDTA (pH 7.4). A discontinuous sucrose gradient [2 M sucrose (1 mL), 1.6 M (2

mL), 1.4 M (4 mL, containing homogenate), 1.2 M (4 mL), and 0.8 M (1 mL)] was centrifuged for 2.5 h at 140,000*g* in an SW 27 rotor to separate PM, Golgi, and endoplasmic reticulum (ER) vesicles, as described (Rossi et al., 2012a). Vesicle size was measured by quasi-elastic light scattering (N5 Submicron Particle Size Analyzer, Beckman) and direct stochastic optical reconstruction microscopy (*d*STORM). For internalization studies, separation of PM from intracellular vesicles was performed by differential centrifugation, as described (Rossi et al., 2012a).

AQP4-Reconstituted Proteoliposomes

Purified recombinant human M1-AQP4 (provided by William Harries and Robert Stroud, UCSF) was reconstituted at 3% (wt/wt) in proteoliposomes containing 95:5 L-α-phosphatidylcholine:L-α-phosphatidylserine by detergent dialysis using β-octyl-glucoside, as described (Tradtrantip et al., 2012).

Electrophoresis

Blue-native polyacrylamide gel electrophoresis (BN/ PAGE) was done as described (Rossi et al., 2012a). Briefly, cells or membrane vesicles were suspended in blue native lysis buffer and incubated for 30 min. Samples were then centrifuged at 22,000*g* for 30 min. Ten micrograms of protein sample was mixed with 5% Coomassie blue G-250 and loaded in each lane. Ferritin was used as the molecular mass standard (440 and 880 kDa). Laemmli SDS/PAGE gels consisted of a 12% running gel and 3% stacking gel. A total of 2.5 μg protein sample was mixed with Laemmli buffer and loaded in each lane.

Immunoblot

Proteins were blotted at 160 mA for 1.5 h onto polyvinylidene difluoride membranes (Millipore) using a native transfer buffer (50 mM tricine and 7.5 mM imidazole) for BN gels or transfer buffer (Invitrogen) for SDS gels. Membranes were blocked with 3% BSA and incubated with the following primary antibodies at 4°C overnight: goat or rabbit anti-AQP4 (Santa Cruz Biotechnology, Santa Cruz, CA), calnexin, *trans*-Golgi network-46, and Na^+/K^+ ATPase (Abcam, Cambridge, MA). Membranes were then rinsed, incubated for 1 h with horseradish peroxidase- conjugated goat anti-rabbit IgG or donkey antigoat IgG (Santa Cruz Biotechnology), rinsed extensively, and labeled proteins were detected using the ECL Plus enzymatic chemiluminescence kit (GE Healthcare).

Quantitative Analysis of NMO-IgG Binding to PM Vesicles

Vesicles containing M23-AQP4, prepared as described above, were immobilized on poly-D-lysine-coated MatTek dishes (MatTek, Ashland, MA) for 1 h, then rinsed with PBS, and incubated at room temperature for 30 min with rAbs or NMO sera. Vesicles were then rinsed with PBS, fixed in 4% paraformaldehyde for 15 min, and permeabilized with 0.1% Triton-X-100. Vesicles were then blocked in PBS containing 6 mM glucose, 1 mM Na-pyruvate (PBS+), and 1% bovine serum albumin (BSA) and incubated for 30 min with 0.4 μg/mL polyclonal, Cterminal- specific rabbit anti-AQP4 antibody (Santa Cruz Biotechnology) and then rinsed with PBS. Vesicles were incubated for 30 min with 4 μg/mL goat anti-human IgG-conjugated Alexa Fluor 555 and goat anti-rabbit IgG-conjugated Alexa Fluor 488 (Invitrogen) in blocking buffer. Antibody binding was quantified by ratio imaging fluorescence microscopy using a Nikon Eclipse TE2000E TIRF microscope equipped with Nikon 100× oil immersion lens, as described (Crane et al., 2011).

Stopped-Flow Measurement of Osmotic Water Permeability

Stopped-flow measurements were done on a Hi-Tech Sf-51 instrument (Hi-Tech Scientific, Bradford-on-Avon, UK). PM vesicles were resuspended at a concentration of 0.5 mg

protein/mL in 250 mM sucrose, 10 mM Tris–HCl, pH 7.4, and were subjected to a 250 mM inwardly directed gradient of sucrose. The kinetics of decreasing vesicle volume was measured from the time course of 90° scattered light intensity at 530 nm wavelength. Osmotic water permeability coefficients (P_f) were computed from the light scattering time course, as described (Yang et al., 1997). NMO or control sera (up to 20%) or NMO rAbs (up to 200 μg/mL) were added to the vesicle or proteoliposome suspension 1 h before stopped-flow experiments.

Total Internal Reflection Fluorescence Microscopy

Total internal reflection fluorescence microscopy (TIRFM) was done using a Nikon Eclipse TE2000E microscope equipped with a through-objective TIRF attachment and a 100× oil immersion objective (numerical aperture 1.49) mounted on a perfect focus module (Nikon, Melville, NY). Fluorescence was imaged using an EM-CCD camera (QuantEM:512SC, Photometrics, Tucson, AZ) using quad-band filter cube (LF405/488/561/ 635-A-NTE, Semrock, Lake Forest, IL) and appropriate emission filters (FF02-520/28-25, FF01-600/37-25, Semrock) mounted on a Lambda 10-3 optical filter changer (Sutter Instruments, Novato, CA). Live-cell time-lapse images of M1-AQP4 conjugated to mCherry (M1- mCherry) and M23-AQP4 conjugated to GFP (M23-GFP) were done over 30 min at 1 frame/s.

Super-Resolution Imaging

*d*STORM using Alexa-labeled Abs and photoactivated localization microscopy (PALM) were performed as described (Rossi et al., in press). Briefly, TIRF image sequences were acquired at 40 Hz and reconstructed using ImageJ plug-in QuickPALM (Henriques et al., 2010). The spatial localization precision was ~20 nm under the measurement conditions here. For live-cell PALM, the laser power for fluorescence excitation was ~1 kW/cm^2 (cw, 561 nm for PAmCherry) to excite fluorescence and cause bleaching. The activation laser was pulsed at 1–20 Hz with pulse duration of 1–10 ms, which was adjusted empirically to provide optimal stochastic activation of fluorophores. For *d*STORM, fluorophore was excited using moderate laser power at 568 nm (Alexa Fluor 568; 3 kW/cm^2). The image processing package Fiji was used to analyze OAP size in reconstructed images.

NMO-IgG Internalization Assay

Cells stably expressing M1- or M23-AQP4 were grown on coverglasses until confluent. Cells were washed twice with PBS+ and incubated for 20 min in PBS+ containing 1% BSA at room temperature. Cells were subsequently labeled with rAb-58-Cy3 (20 μg/mL) at 4°C for 1 h. Following extensive washing with cold PBS+, cells were chased at 37°C for 1 h. Coverglasses were mounted in an open chamber and fluorescence was measured using an inverted epifluorescence microscope (Eclipse TE2000-E, Nikon) with a Nikon oil immersion 100×, NA 1.49 Apo TIRF objective lens. Fluorescence images were obtained before and after addition of the dark quencher bromocresol green (final concentration 4 mM) in the cellbathing solution, as described (Ratelade et al., 2011). The fraction of internalized antibody was determined as the (background-subtracted) ratio of the fluorescence signal after vs. before quencher addition.

Quantification of Cell Surface AQP4

AQP4-transfected cells were grown on coverglasses until confluent and incubated for specified times with 50 μg/mL rAb-58 at 37°C. Cells were then washed extensively in cold PBS+ and blocked for 20 min in 1% BSA at 4°C. Remaining AQP4 at the cell surface was labeled with 50 μg/mL rAb-58 at 4°C for 1 h. Subsequently, rAb-58 was labeled by incubation for 1 h at 4°C with goat anti-human IgG-conjugated Alexa Fluor 555 (1:200,

Invitrogen) and the PM was stained using a fluorescent lectin, Wheat Germ Agglutinin-conjugated Alexa Fluor 488 (1:400, Invitrogen). Cells were then washed in cold PBS+ and fixed for 15 min in 4% PFA. Surface AQP4 was quantified as the ratio of red (surface AQP4) to green (PM) fluorescence using FiJi software.

RESULTS

NMO-IgG Does Not Inhibit AQP4 Water Permeability

CHO cells were stably transfected with M1- or M23- AQP4 and characterized by imaging and biochemical methods (Fig. 1). By confocal fluorescence microscopy, both isoforms showed a PM pattern, which was smooth for M1-AQP4 and punctate for M23-AQP4 (Fig. 1A, top), reflecting their different oligomeric states. TIRFM confirmed AQP4 clustering in OAPs at the PM of cells expressing M23- but not M1-AQP4 (Fig. 1A, middle). Super-resolution imaging by *d*STORM showed small puncta in cells expressing M1-AQP4 with an average diameter of 27 ± 11 nm (SD), which is near the spatial resolution limit of *d*STORM, whereas M23-AQP4-expressing cells showed large clusters of average diameter of 117 ± 45 nm, with considerable heterogeneity in size (Fig. 1A, bottom). SDS/PAGE and AQP4 immunoblot showed the expected molecular sizes of M1- and M23- AQP4 (Fig. 1B, top). Assembly of M23-AQP4 in OAPs was confirmed by BN/PAGE in which multiple bands were seen (Fig. 1B, bottom), whereas M1-AQP4 was present as a single major band.

To measure water permeability, PM vesicles were isolated from CHO cells expressing M1- or M23-AQP4 (and from nontransfected cells). Fractions enriched in PMs, ER, and Golgi were prepared by sucrose-density gradient centrifugation (Fig. 2A, left). The purity of each fraction was verified by SDS/PAGE and immunoblot analysis using Na^+/K^+ ATPase (PM), *trans*-Golgi network-46 (TGN-46; Golgi), and calnexin (ER) as markers (Fig. 2A, right). M1- and M23-AQP4 were detected only in the PM fraction. By BN/PAGE and AQP4 immunoblot, M23-AQP4 was seen as high-molecular- weight bands, representing OAPs, whereas M1- AQP4 was seen mainly as a band of lower molecular size corresponding to tetramers (Fig. 2B). By quasi-elastic light scattering, the size distributions of vesicles containing M1- and M23-AQP4 were similar, with average diameters of 263 ± 41 and 247 ± 55 nm (SD), respectively (Fig. 2C, top). *d*STORM of surface-immobilized PM vesicles stained with an anti-C-terminus AQP4 antibody showed average diameters of 252 ± 61 and 239 ± 65 nm (SD) (Fig. 2C, bottom), in agreement with the quasi-elastic light scattering data.

Osmotic water permeability in the PM vesicles was measured by stopped-flow light scattering from the kinetics of vesicle shrinking in response to an osmotic gradient. Figure 2D (left) shows light scattering data from vesicles from nontransfected cells (labeled “no AQP4") and from M1- and M23-AQP4-expressing cells. Osmotic equilibration was much faster ($t_{1/2}$ ~0.4 s) for AQP4-containing vesicles than for control vesicles ($t_{1/2}$ ~2.9 s). Figure 2D (right) summarizes relative single-molecule water permeability, which did not differ significantly for M1- and M23-AQP4, indicating that AQP4 clustering in OAPs does not affect its intrinsic water permeability.

To confirm tight binding of NMO-IgG to AQP4 in PM vesicles, M23-AQP4-containing vesicles were immobilized on a cover glass and incubated with NMO-IgG followed by a red fluorescent anti-human secondary antibody. Binding was normalized to AQP4 expression by ratio imaging using an antibody against the AQP4 C-terminus conjugated with a green fluorescent secondary antibody. Figure 3A shows representative fluorescence micrographs for an NMO serum specimen (10%) and a recombinant NMO-IgG rAb-53 (200 μg/mL). Figure 3B (left) shows binding curves as red-to-green (R/G) fluorescence ratios as a function of serum or rAb concentration. For subsequent experiments, high concentrations of serum

(10%) and rAbs (200 μg/mL) were used in which binding to AQP4 was saturated. Figure 3B (right) shows R/G ratios for six NMO sera (each at 10%) and two NMO-rAbs (rAb-53 and rAb-58, each at 200 μg/mL). We also included AQmab, which is a mutated rAb-53 with deleted effector function (Tradtrantip et al., 2012).

Osmotic water permeability of the M23-AQP4-containing PM vesicles (M23-vesicles) was measured following incubation with sera or rAbs under conditions of saturated binding (Fig. 3C). NMO-IgG from NMO sera, NMO-rAbs, or AQmab did not significantly alter AQP4 water permeability. Osmotic water permeability measurements were also done using M1-AQP4-reconstituted proteoliposomes (M1-proteoliposomes) (Fig. 3D). Although AQP4 reconstitution greatly increased liposome water permeability, there was no significant effect of NMO-IgG incubation.

NMO-IgG Causes More Rapid Internalization of M23-AQP4 than M1-AQP4 When Expressed Separately in Transfected Cells

To study a potential differential effect of NMO-IgG on endocytosis of M1- vs. M23-AQP4, we used monoclonal recombinant NMO antibody rAb-58, which binds both isoforms with comparable affinity (Crane et al., 2011). CHO cells expressing M1- or M23-AQP4 were labeled with rAb-58 conjugated to the red fluorophore Cy3 (rAb-58-Cy3) for 1 h at 4°C. Endocytosis does not occur at 4°C. Cells were washed extensively and chased at 37°C for 1 h to allow internalization of rAb-58-Cy3 and its target AQP4. Fluorescence of antibody remaining at the cell surface was quenched by addition of the cell-impermeable dark quencher bromocresol green, allowing quantitative determination of the percentage of internalized rAb-58- Cy3. Figure 4A shows rAb-58-Cy3 fluorescence at 0 and 1 h chase time, before vs. after quencher addition. At 0 h rAb-58-Cy3 was present exclusively at the cell surface, as seen by the membrane expression pattern and loss of fluorescence upon addition of quencher. Binding was AQP4 dependent, as no fluorescence was seen in nontransfected cells (data not shown). At 1 h the majority of rAb-58-Cy3 was internalized, as seen by the minimal effect of quencher addition. Figure 4A (right) shows 75 and 92% internalization of rAb-58-Cy3 in M1- and M23-AQP4- expressing cells, respectively.

Figure 4B (left) shows staining of surface AQP4 (red) in CHO cells expressing M1- or M23-AQP4 after 0 or 1 h incubation at 37°C with NMO-IgG (rAb-58). Decreased cell surface AQP4 expression was seen for both AQP4 isoforms, with little change for control (non-NMO) IgG. Surface AQP4 was quantified by the ratio of red (AQP4) to green (PM labeled with the lectin WGA) fluorescence. Figure 4B (right) shows that 71% of M1-AQP4 and 41% of M23-AQP4 remained at the cell surface at 1 h after NMO-IgG exposure. Greater internalization of M23- vs. M1-AQP4 was also seen in the astrocytoma cell line U87MG (Fig. 4B, right).

Endocytosis of M23-AQP4 in OAPs was visualized in live cells by TIRFM. U87MG cells were transfected with the chimeric protein M23-GFP, with GFP at the AQP4 C-terminus. Supporting Information Movie 1 shows GFP internalization at 37°C following addition of rAb-58, with selected frames shown in Fig. 4C. Distinct OAPs composed of M23-AQP4 were seen. Distinct, random endocytic events were seen as disappearance of individual OAPs (arrowheads in Fig. 4C). OAP disappearance was an all-or-none event. Together, the data indicate efficient internalization of M23-AQP4 in transfected cells at a greater rate than M1-AQP4.

NMO-IgG Causes Simultaneous Cointernalization of M1- and M23-AQP4 When Both Isoforms Are Coexpressed in OAPs in Transfected Cells

We also investigated internalization of M1- and M23- AQP4 when both isoforms are coexpressed. CHO cells were transiently transfected with a vector giving comparable expression of M1- and M23-AQP4 in the same cells. PM and intracellular AQP4 were quantified by subcellular fractionation and immunoblot after 2 h incubation with NMO-IgG (rAb-58) at 37°C. Figure 5A (left) shows AQP4 mainly in the PM fraction following incubation with control (non-NMO) IgG, with approximately equal amounts of M1- and M23-AQP4. Approximately 50% of M1- and M23-AQP4 remained in the PM fraction after 2 h incubation with NMO-IgG. In contrast, ~10% of M23-AQP4 remained in the PM fraction at 2 h in cells expressing M23-AQP4 alone. Figure 5A (right) summarizes PM and cytosolic amounts of AQP4 after 2 h exposure to control (non-NMO) IgG or NMO-IgG (rAb-58). These biochemical data were confirmed by immunofluorescence of cell surface AQP4. Figure 5B (left) shows staining of surface AQP4 in cells coexpressing M1- and M23-AQP4 or M23-AQP4 alone and incubated for 2 h with NMO-IgG at 37°C. In agreement with the fractionation data, ~55% of AQP4 remained at the cell surface in cells coexpressing M1- and M23-AQP4 compared with ~15% for M23-AQP4 alone (Fig. 5B, right).

Live-cell TIRFM was done to visualize the real-time dynamics of internalization of M1- and M23-AQP4. U87MG cells were cotransfected with M1-mCherry (red fluorescent) and M23-GFP (green fluorescent). Figure 5C shows that red and green fluorescence colocalized in OAPs, indicating comingling of both isoforms as predicted from prior studies (Jin et al., 2011; Neely et al., 1999; Rossi et al., in press; Tajima et al., 2010). Supporting Information Movie 2 shows real-time, two-color TIRFM following exposure of cells to NMO-IgG, with selected frames provided in Fig. 5C. Distinct endocytic events were seen as disappearance of individual OAPs with simultaneous loss of red and green fluorescence (arrowheads in Fig. 5C). NMO-IgG thus causes simultaneous internalization of M1- and M23-AQP4.

NMO-IgG Does Not Cause AQP4 Cell Surface Clustering

Super-resolution imaging (live-cell PALM) was done to quantify OAP size in cells coexpressing M1- and M23-AQP4, both of which were expressed as C-terminus chimeras with the photoactivatable protein PAmCherry. Cells were imaged before and at 45 min after NMO-IgG (20% serum) incubation (Fig. 6A). PALM image reconstructions show distinct OAPs, most with diameters of 40–75 nm, similar to those seen in astrocytes (Rossi et al., in press). OAPs were similar in size after NMO-IgG exposure, though fewer in number because of endocytosis. Quantitative analysis of OAP area showed no significant effect of NMO-IgG exposure (Fig. 6B). Using *d*STORM in fixed cells, we previously showed no effect of NMO-IgG on OAP size in primary astrocyte cultures, which natively coexpress M1- and M23-AQP4 in similar quantities (Rossi et al., in press).

N-Terminus GFP Insertion Disrupts M23-AQP4 OAPs

We previously reported that OAP formation by M23- AQP4 is stabilized by hydrophobic intermolecular interactions involving N-terminus residues just downstream of Met-23, and that the absence of OAPs in M1-AQP4 results from nonselective blocking of this interaction by residues upstream of Met-23 (Crane and Verkman, 2009). We therefore speculated that a problem with the Hinson et al. (2012) study was that their M23-GFP chimera with GFP insertion at the AQP4 N-terminus could not form OAPs. Figure 7 (left panels) shows the sites of GFP insertion at the AQP4 N-terminus ($AQP4_NGFP$) and C-terminus ($AQP4_CGFP$). TIRFM (center panels) shows that the M23-AQP4 ($M23_NGFP$) chimera containing GFP at its N-terminus had a smooth fluorescence pattern, similar to $M1_NGFP$, whereas the C-terminus $M23_CGFP$ chimera showed punctate fluorescence, with the $M1_CGFP$ chimera showing smooth fluorescence. Therefore, the C-terminus GFP insertion does not interfere

with AQP4 supramolecular assembly, in agreement with previous results (Pisani et al., 2011; Rossi et al., in press; Tajima et al., 2010), whereas the N-terminus GFP insertion prevents OAP formation by M23-AQP4. BN/PAGE (right panels) confirmed this conclusion.

DISCUSSION

Major questions in NMO pathogenesis include the cause of NMO-IgG autoimmunity, how NMO-IgG enters the CNS, and, once in the CNS, how it causes pathology. Evidence from cell culture (Kalluri et al., 2010; Phuan et al., 2012), organ culture (Zhang et al., 2011), and mouse (Saadoun et al., 2010) models, and from the pathology of human NMO lesions (Lucchinetti et al., 2002), suggests that complement plays a central role in NMO pathogenesis involving CDC and astrocyte damage, which is speculated to cause cytokine release, disruption of the blood–brain barrier, recruitment of granulocytes and macrophages, and, ultimately, death of oligodendrocytes and neurons (Papadopoulos and Verkman, 2012). An alternative model of NMO pathogenesis was suggested by Hinson et al. (2008), who reported that NMO-IgG causes rapid internalization of AQP4 and the excitatory amino acid transporter 2 (EAAT2) in astrocytes, resulting in elevated extracellular space glutamate and consequent excitotoxicity. We previously challenged this model, reporting lack of significant EAAT2 internalization or reduced glutamate transport in astrocyte cultures exposed to NMO-IgG and little AQP4 internalization in astrocytes *in vivo* (Ratelade et al., 2011). Conceptually, the internalization model is difficult to reconcile with the fact that continued AQP4 exposure is necessary for NMO-IgG binding and CDC, so that AQP4 internalization would be protective rather than pathogenic. Here, we critically examined a recent model from the same group (Hinson et al., 2012) based on AQP4 water transport inhibition by NMO-IgG and preferential internalization of M1-AQP4, which produces a M23- AQP4-enriched pool of clustered PM AQP4, resulting in enhanced CDC and local tissue swelling. Our data challenge each of the major conclusions of Hinson et al. (2012) as well as their logic supporting their model.

Whether NMO-IgG inhibits AQP4 water permeability is important, as AQP4 knockout mice, when appropriately stressed, manifest abnormalities in brain water balance (Manley et al., 2000; Papadopoulos et al., 2004), neuroexcitation (Binder et al., 2006), astrocyte migration (Auguste et al., 2007; Saadoun et al., 2005), and neuroinflammation (Li et al., 2011). The literature on AQP4 water permeability has been confusing because of challenges in water permeability measurement, which requires accurate, quantitative determination of rapid changes in cell volume in response to osmotic gradients. For example, several classes of drugs, including carbonic acid inhibitors and antiepileptics, were reported to inhibit AQP4 water permeability (Huber et al., 2007, 2009), but shown subsequently to lack inhibition activity (Yang et al., 2008). Studies of the intrinsic (single-molecule) AQP4 water permeability of M1-AQP4 tetramers vs. M23-AQP4 OAPs have produced widely discordant results, with relative M1-AQP4 water permeability higher than M23-AQP4 (Fenton et al., 2010) and lower than M23-AQP4 (Silberstein et al., 2004). The Hinson et al. (2012) study used time-to-bursting of Xenopus oocytes in a hypo-osmolar buffer as a measure of water permeability. This is an inaccurate surrogate of *bona fide* water permeability, as time-to-bursting depends on oocyte physical properties as well as the activity of various ion channel and solute transporters, which are quite variable and can be affected by environmental factors, antibody binding, etc. In our original description of oocyte water permeability measurement (Zhang et al., 1990) as subsequently refined by Zeuthen et al. (2007), it was concluded that meaningful measurements require quantitative oocyte volume determinations just after osmotic challenge with time resolution of 1 s or better.

We found no significant inhibition of AQP4 water permeability by high concentrations of serum from multiple NMO patients as well as monoclonal NMO antibodies. Saturation of

NMO-IgG binding to AQP4 was confirmed, and water permeability was measured by a stopped-flow light scattering method with mixing time <1 ms, which quantifies water permeability with high accuracy and without the potentially confounding effects of internalization (as occurs in cell culture studies), unstirred layers, and ion/solute transport. In addition, NMO-IgG did not reduce osmotic water permeability in proteoliposomes reconstituted with purified recombinant AQP4. As our measurements are sensitive to <5% changes in water permeability, we conclude that NMO-IgG does not inhibit AQP4 water permeability to a biologically relevant extent. This conclusion is not unexpected, as the large size of NMO-IgG compared with AQP4 precludes binding of more than one NMO-IgG per AQP4 tetramer, which contain four monomers with separate water pores (Ho et al., 2009). Inhibition of a water pore likely requires a high degree of steric blockade that is unlikely to be conferred by an antibody. Lastly, we note that two prior studies have also concluded that NMO-IgG does not inhibit AQP4 water permeability (Melamud et al., 2012; Nicchia et al., 2009), though these studies involved measurements on cell cultures where solution mixing time and measurement accuracy limited their ability to detect small differences in water permeability.

We found here that M1- and M23-AQP4 have similar single-molecule water permeability. Our measurements were done by stopped-flow light scattering on PM vesicles, taking into account vesicle size and AQP4 content for computation of single-molecule water permeability. OAP formation by M23-AQP4 was confirmed, indicating that AQP4 supramolecular assembly does not influence its single-molecule water permeability, which is not unexpected, as the AQP4 aqueous pore is located near the center of each monomer (Ho et al., 2009). The biological role of AQP4 supramolecular assembly thus remains unclear. An alternative possible role in cell–cell adhesion, which was proposed from electron crystallography structural analysis (Hiroaki et al., 2006), was not confirmed experimentally (Zhang and Verkman, 2008). Perhaps, AQP4 supramolecular assembly is involved in maintaining its efficient polarization to astrocyte foot processes at endothelial cell contacts, though the unaffected blood–brain barrier anatomy and function in AQP4 knockout mice (Manley et al., 2000; Papadopoulos and Verkman, 2005; Saadoun et al., 2009) argue against this possibility.

Hinson et al. (2012) reported that M23-AQP4 is resistant to endocytic internalization, postulating that the large size of OAPs prevents their incorporation into clathrin- coated pits and endosomes. The consequences of differential internalization of M1- and M23-AQP4 would include progressive enrichment of M23-AQP4 in the PM and increased OAP size. Contradictory to the conclusions of Hinson et al. (2012), we found that M23-AQP4 in cell cultures was internalized following NMO-IgG binding at a greater rate than M1-AQP4. The more rapid internalization of M23-AQP4 may be a consequence of bivalent NMO-IgG binding to M23-AQP4 in OAPs, as it has been shown previously that binding of an Fab fragment to its antigen does not cause internalization (Hughes et al., 2010). Live-cell video imaging showed rapid internalization of M23-AQP4 OAPs whose size (diameter ~110 nm) is greater than that of OAPs in astrocytes (diameter ~45 nm). These values are substantially less than the diameter of ~200 nm of a nascent endosome. We reported recently that large OAPs formed by M23-AQP4 remain intact unless cell membrane curvature is very high (vesicle diameter <110 nm) (Rossi et al., 2012a) and show here that OAP formation by M23- AQP4 is unimpaired in PM vesicles of diameter ~250 nm. The possibility of differential internalization of M1- and M23-AQP4 was also tested in cells expressing both isoforms in which NMO-IgG was added to induce internalization. We found that M1- and M23-AQP4 are internalized together in individual clusters and that differential internalization does not occur. This result is not unexpected, as M1-AQP4 and M23-AQP4 comingle in stable OAPs that are not easily dissociated (Jin et al., 2011; Neely et al., 1999; Rossi et al., in press; Tajima et al., 2010).

We reported previously that little if any NMO-IgG or AQP4 internalization occurs in astrocytes in mouse brain *in vivo*, in which NMO-IgG was administered by direct intraparenchymal injection (Ratelade et al., 2011). Under the same conditions, other astrocyte endosomal markers such as sulforhodamine 101 and Texas Red-dextran were efficiently internalized. We postulate that the unique polarized expression of AQP4 in astrocyte foot processes may be responsible for the different results in transfected cell cultures. Conflicting results have been reported in astrocyte culture models, which may be related to their different states of differentiation. Finally, it is unlikely that reduced AQP4 water permeability in astrocytes, even if it occurred as a result of NMO-IgG binding, would cause astrocytic edema or intramyelinic edema. Edema is not seen at baseline in AQP4 knockout mice (Manley et al., 2000; Papadopoulos and Verkman, 2005; Saadoun et al., 2009) or in mice administrated large amounts of NMO-IgG by intraparenchymal injection (Saadoun et al., 2010). Oligodendrocytes do not express AQP4 and therefore reduced AQP4 water permeability in astrocytes could not produce intramyelinic edema. Astrocytic and intramyelinic edema are nonspecific findings seen in many other CNS diseases in the absence of NMO-IgG (Balbi et al., 2010). Astrocytic edema is found in cerebral ischemia (Steiner et al., 2012) and intramyelinic edema in metabolic abnormalities (phenylketonuria, tyrosinemia, maple syrup urine disease, vitamin B12 deficiency, and central pontine myelinolysis; Anderson and Leuzzi, 2010; Kilicarslan et al., 2012; Ramaekers et al., 1997; Scalabrino, 2005; Sener, 2005).

In conclusion, our results provide experimental evidence against NMO-IgG-induced: (i) inhibition of AQP4 water permeability, (ii) preferential M1-AQP4 internalization, and (iii) OAP clustering, and hence the validity of the model of NMO pathogenesis proposed by Hinson et al. (2012). The clustering observed by Hinson et al. (2012) may be a nonspecific effect of cytotoxicity as it has been found for other toxic insults to astrocytes (Anders and Brightman, 1982) and may be related to cell membrane crowding or altered membrane composition or protein–protein interactions. Further, AQP4 clustering is unlikely to increase CDC because all but the smallest OAPs produce comparable CDC when normalized to the number of AQP4 tetramers (Phuan et al., 2012). Finally, it is unlikely that reduced AQP4 water permeability, even if it occurred, would cause cellular or intramyelinic edema. Lastly, we note that neither NMOIgG inhibition of AQP4 water permeability nor enhanced M1-AQP4 internalization is important or necessary for the current working model of NMO pathogenesis, which involves NMO-IgG binding to astrocyte AQP4, astrocyte cytotoxicity, inflammation, and demyelination.

Acknowledgments

Grant sponsor: National Institutes of Health; Grant number: EY13574, EB00415, DK35124, HL73856, DK86125, DK72517; Guthy-Jackson Charitable Foundation.

Abbreviations

AQmab	aquaporumab
AQP4	aquaporin-4
BN/PAGE	blue-native polyacrylamide gel electrophoresis
CDC	complement-dependent cytotoxicity
CNS	central nervous system
***d*STORM**	direct stochastic optical reconstruction microscopy
EAAT2	excitatory amino acid transporter 2

GFP	green fluorescent protein
NMO	neuromyelitis optica
NMO-IgG	neuromyelitis optica immunoglobulin G
OAPs	orthogonal arrays of particles
PALM	photoactivated localization microscopy
PAmCherry	photoactivatable mCherry
rAb	recombinant monoclonal antibody
TIRFM	total internal reflection fluorescence microscopy.

REFERENCES

Anders JJ, Brightman MW. Particle assemblies in astrocytic plasma membranes are rearranged by various agents in vitro and cold injury in vivo. J Neurocytol. 1982; 11:1009–1029. [PubMed: 7153786]

Anderson PJ, Leuzzi V. White matter pathology in phenylketonuria. Mol Genet Metab. 2010; 1:3–9.

Auguste KI, Jin S, Uchida K, Yan D, Manley GT, Papadopoulos MC, Verkman AS. Greatly impaired migration of implanted aquaporin-4-deficient astroglial cells in mouse brain toward a site of injury. FASEB J. 2007; 21:108–116. [PubMed: 17135365]

Balbi P, Salvini S, Fundaro C, Frazzitta G, Maestri R, Mosah D, Uggetti C, Sechi G. The clinical spectrum of late-onset Alexander disease: A systematic literature review. J Neurol. 2010; 257:1955–1962. [PubMed: 20721574]

Bennett JL, Lam C, Kalluri SR, Saikali P, Bautista K, Dupree C, Glogowska M, Case D, Antel JP, Owens GP, Gilden D, Nessler S, Stadelmann C, Hemmer B. Intrathecal pathogenic anti-aquaporin-4 antibodies in early neuromyelitis optica. Ann Neurol. 2009; 66:617–629. [PubMed: 19938104]

Binder DK, Yao X, Zador Z, Sick TJ, Verkman AS, Manley GT. Increased seizure duration and slowed potassium kinetics in mice lacking aquaporin-4 water channels. Glia. 2006; 53:631–636. [PubMed: 16470808]

Bradl M, Misu T, Takahashi T, Watanabe M, Mader S, Reindl M, Adzemovic M, Bauer J, Berger T, Fujihara K, Itoyama Y, Lassmann H. Neuromyelitis optica: Pathogenicity of patient immunoglobulin in vivo. Ann Neurol. 2009; 66:630–643. [PubMed: 19937948]

Brenner M, Johnson AB, Boespflug-Tanguy O, Rodriguez D, Goldman JE, Messing A. Mutations in GFAP, encoding glial fibrillary acidic protein, are associated with Alexander disease. Nat Genet. 2001; 27:117–120. [PubMed: 11138011]

Crane JM, Lam C, Rossi A, Gupta T, Bennett JL, Verkman AS. Binding affinity and specificity of neuromyelitis optica autoantibodies to aquaporin-4 M1/M23 isoforms and orthogonal arrays. J Biol Chem. 2011; 286:16516–16524. [PubMed: 21454592]

Crane JM, Verkman AS. Determinants of aquaporin-4 assembly in orthogonal arrays revealed by live-cell single-molecule fluorescence imaging. J Cell Sci. 2009; 122:813–821. [PubMed: 19240114]

Fenton RA, Moeller HB, Zelenina M, Snaebjornsson MT, Holen T, Mac-Aulay N. Differential water permeability and regulation of three aquaporin 4 isoforms. Cell Mol Life Sci. 2010; 67:829–840. [PubMed: 20013023]

Henriques R, Lelek M, Fornasiero EF, Valtorta F, Zimmer C, Mhlanga MM. QuickPALM: 3D real-time photoactivation nanoscopy image processing in ImageJ. Nat Methods. 2010; 7:339–340. [PubMed: 20431545]

Hinson SR, Roemer SF, Lucchinetti CF, Fryer JP, Kryzer TJ, Chamberlain JL, Howe CL, Pittock SJ, Lennon VA. Aquaporin-4-binding autoantibodies in patients with neuromyelitis optica impair glutamate transport by down-regulating EAAT2. J Exp Med. 2008; 205:2473–2481. [PubMed: 18838545]

Hinson SR, Romero MF, Popescu BF, Lucchinetti CF, Fryer JP, Wolburg H, Fallier-Becker P, Noell S, Lennon VA. Molecular outcomes of neuromyelitis optica (NMO)-IgG binding to aquaporin-4 in astrocytes. Proc Natl Acad Sci USA. 2012; 109:1245–1250. [PubMed: 22128336]

Hiroaki Y, Tani K, Kamegawa A, Gyobu N, Nishikawa K, Suzuki H, Walz T, Sasaki S, Mitsuoka K, Kimura K, Mizoguchi A, Fujiyoshi Y. Implications of the aquaporin-4 structure on array formation and cell adhesion. J Mol Biol. 2006; 355:628–639. [PubMed: 16325200]

Ho JD, Yeh R, Sandstrom A, Chorny I, Harries WE, Robbins RA, Miercke LJ, Stroud RM. Crystal structure of human aquaporin 4 at 1.8 A and its mechanism of conductance. Proc Natl Acad Sci USA. 2009; 106:7437–7442. [PubMed: 19383790]

Huber VJ, Tsujita M, Kwee IL, Nakada T. Inhibition of aquaporin 4 by antiepileptic drugs. Bioorg Med Chem. 2009; 17:418–424. [PubMed: 18178093]

Huber VJ, Tsujita M, Yamazaki M, Sakimura K, Nakada T. Identification of arylsulfonamides as aquaporin 4 inhibitors. Bioorg Med Chem Lett. 2007; 17:1270–1273. [PubMed: 17178220]

Hughes EG, Peng X, Gleichman AJ, Lai M, Zhou L, Tsou R, Parsons TD, Lynch DR, Dalmau J, Balice-Gordon RJ. Cellular and synaptic mechanisms of anti-NMDA receptor encephalitis. J Neurosci. 2010; 30:5866–5875. [PubMed: 20427647]

Jarius S, Wildemann B. AQP4 antibodies in neuromyelitis optica: Diagnostic and pathogenetic relevance. Nat Rev Neurol. 2010; 6:383–392. [PubMed: 20639914]

Jin BJ, Rossi A, Verkman AS. Model of aquaporin-4 supramolecular assembly in orthogonal arrays based on heterotetrameric association of M1/M23 isoforms. Biophys J. 2011; 100:2936–2945. [PubMed: 21689527]

Kalluri SR, Illes Z, Srivastava R, Cree B, Menge T, Bennett JL, Berthele A, Hemmer B. Quantification and functional characterization of antibodies to native aquaporin 4 in neuromyelitis optica. Arch Neurol. 2010; 67:1201–1208. [PubMed: 20937947]

Kilicarslan R, Alkan A, Demirkol D, Toprak H, Sharifov R. Maple syrup urine disease: Diffusion-weighted MRI findings during acute metabolic encephalopathic crisis. Jpn J Radiol. 2012; 30:522–525. [PubMed: 22476847]

Kinoshita M, Nakatsuji Y, Kimura T, Moriya M, Takata K, Okuno T, Kumanogoh A, Kajiyama K, Yoshikawa H, Sakoda S. Neuromyelitis optica: Passive transfer to rats by human immunoglobulin. Biochem Biophys Res Commun. 2009; 386:623–627. [PubMed: 19545538]

Lennon VA, Kryzer TJ, Pittock SJ, Verkman AS, Hinson SR. IgG marker of optic-spinal multiple sclerosis binds to the aquaporin-4 water channel. J Exp Med. 2005; 202:473–477. [PubMed: 16087714]

Li L, Zhang H, Varrin-Doyer M, Zamvil SS, Verkman AS. Proinflammatory role of aquaporin-4 in autoimmune neuroinflammation. FASEB J. 2011; 25:1556–1566. [PubMed: 21257712]

Lucchinetti CF, Mandler RN, McGavern D, Bruck W, Gleich G, Ransohoff RM, Trebst C, Weinshenker B, Wingerchuk D, Parisi JE, Lassmann H. A role for humoral mechanisms in the pathogenesis of Devic's neuromyelitis optica. Brain. 2002; 125:1450–1461. [PubMed: 12076996]

Manley GT, Fujimura M, Ma T, Noshita N, Filiz F, Bollen AW, Chan P, Verkman AS. Aquaporin-4 deletion in mice reduces brain edema after acute water intoxication and ischemic stroke. Nat Med. 2000; 6:159–163. [PubMed: 10655103]

Melamud L, Fernandez JM, Rivarola V, Di Giusto G, Ford P, Villa A, Capurro C. Neuromyelitis optica immunoglobulin G present in sera from neuromyelitis optica patients affects aquaporin-4 expression and water permeability of the astrocyte plasma membrane. J Neurosci Res. 2012; 90:1240–1248. [PubMed: 22354518]

Misu T, Fujihara K, Kakita A, Konno H, Nakamura M, Watanabe S, Takahashi T, Nakashima I, Takahashi H, Itoyama Y. Loss of aquaporin 4 in lesions of neuromyelitis optica: Distinction from multiple sclerosis. Brain. 2007; 130:1224–1234. [PubMed: 17405762]

Neely JD, Christensen BM, Nielsen S, Agre P. Heterotetrameric composition of aquaporin-4 water channels. Biochemistry. 1999; 38:11156–11163. [PubMed: 10460172]

Nicchia GP, Mastrototaro M, Rossi A, Pisani F, Tortorella C, Ruggieri M, Lia A, Trojano M, Frigeri A, Svelto M. Aquaporin-4 orthogonal arrays of particles are the target for neuromyelitis optica autoantibodies. Glia. 2009; 57:1363–1373. [PubMed: 19229993]

Nielsen S, Nagelhus EA, Amiry-Moghaddam M, Bourque C, Agre P, Ottersen OP. Specialized membrane domains for water transport in glial cells: High-resolution immunogold cytochemistry of aquaporin-4 in rat brain. J Neurosci. 1997; 17:171–180. [PubMed: 8987746]

Papadopoulos MC, Manley GT, Krishna S, Verkman AS. Aquaporin-4 facilitates reabsorption of excess fluid in vasogenic brain edema. FASEB J. 2004; 18:1291–1293. [PubMed: 15208268]

Papadopoulos MC, Verkman AS. Aquaporin-4 gene disruption in mice reduces brain swelling and mortality in pneumococcal meningitis. J Biol Chem. 2005; 280:13906–13912. [PubMed: 15695511]

Papadopoulos MC, Verkman AS. Aquaporin 4 and neuromyelitis optica. Lancet Neurol. 2012; 11:535–544. [PubMed: 22608667]

Parratt JD, Prineas JW. Neuromyelitis optica: A demyelinating disease characterized by acute destruction and regeneration of perivascular astrocytes. Mult Scler. 2010; 16:1156–1172. [PubMed: 20823059]

Phuan PW, Ratelade J, Rossi A, Tradtrantip L, Verkman AS. Complement-dependent cytotoxicity in neuromyelitis optica requires aquaporin-4 protein assembly in orthogonal arrays. J Biol Chem. 2012; 287:13829–13839. [PubMed: 22393049]

Pisani F, Mastrototaro M, Rossi A, Nicchia GP, Tortorella C, Ruggieri M, Trojano M, Frigeri A, Svelto M. Identification of two major conformational aquaporin-4 epitopes for neuromyelitis optica autoantibody binding. J Biol Chem. 2011; 286:9216–9224. [PubMed: 21212277]

Ramaekers VT, Reul J, Kusenbach G, Thron A, Heimann G. Central pontine myelinolysis associated with acquired folate depletion. Neuropediatrics. 1997; 28:126–130. [PubMed: 9208415]

Rash JE, Yasumura T, Hudson CS, Agre P, Nielsen S. Direct immunogold labeling of aquaporin-4 in square arrays of astrocyte and ependymocyte plasma membranes in rat brain and spinal cord. Proc Natl Acad Sci USA. 1998; 95:11981–11986. [PubMed: 9751776]

Ratelade J, Bennett JL, Verkman AS. Evidence against cellular internalization in vivo of NMO-IgG, aquaporin-4, and excitatory amino acid transporter 2 in neuromyelitis optica. J Biol Chem. 2011; 286:45156–45164. [PubMed: 22069320]

Roemer SF, Parisi JE, Lennon VA, Benarroch EE, Lassmann H, Bruck W, Mandler RN, Weinshenker BG, Pittock SJ, Wingerchuk DM, Pittock SJ, Wingerchuk DM, Lucchinetti CF. Pattern-specific loss of aquaporin-4 immunoreactivity distinguishes neuromyelitis optica from multiple sclerosis. Brain. 2007; 130:1194–1205. [PubMed: 17282996]

Rossi A, Baumgart F, van Hoek AN, Verkman AS. Post-Golgi supramolecular assembly of aquaporin-4 in orthogonal arrays. Traffic. 2012a; 13:43–53. [PubMed: 21981006]

Rossi A, Moritz T, Ratelade J, Verkman AS. Super-resolution imaging of aquaporin-4 orthogonal arrays of particles in cell membranes. J Cell Sci. in press.

Rossi A, Ratelade J, Papadopoulos MC, Bennett JL, Verkman AS. Consequences of NMO-IgG binding to aquaporin-4 in neuromyelitis optica. Proc Natl Acad Sci USA. 2012b; 109:e1511. [PubMed: 22589299]

Saadoun S, Papadopoulos MC, Watanabe H, Yan D, Manley GT, Verkman AS. Involvement of aquaporin-4 in astroglial cell migration and glial scar formation. J Cell Sci. 2005; 118:5691–5698. [PubMed: 16303850]

Saadoun S, Tait MJ, Reza A, Davies DC, Bell BA, Verkman AS, Papadopoulos MC. AQP4 gene deletion in mice does not alter bloodbrain barrier integrity or brain morphology. Neuroscience. 2009; 161:764–772. [PubMed: 19345723]

Saadoun S, Waters P, Bell BA, Vincent A, Verkman AS, Papadopoulos MC. Intra-cerebral injection of neuromyelitis optica immunoglobulin G and human complement produces neuromyelitis optica lesions in mice. Brain. 2010; 133:349–361. [PubMed: 20047900]

Scalabrino G. Cobalamin (vitamin B12) in subacute combined degeneration and beyond: Traditional interpretations and novel theories. Exp Neurol. 2005; 192:463–479. [PubMed: 15755562]

Sener RN. Tyrosinemia: Computed tomography, magnetic resonance imaging, diffusion magnetic resonance imaging, and proton spectroscopy findings in the brain. J Comp Assist Tomogr. 2005; 29:323–325.

Silberstein C, Bouley R, Huang Y, Fang P, Pastor-Soler N, Brown D, Van Hoek AN. Membrane organization and function of M1 and M23 isoforms of aquaporin-4 in epithelial cells. Am J Physiol Renal Physiol. 2004; 287:501–511.

Steiner E, Enzmann GU, Lin S, Ghavampour S, Hannocks MJ, Zuber B, R€uegg MA, Sorokin L, Engelhardt B. Loss of astrocyte polarization upon transient focal brain ischemia as a possible mechanism to counteract early edema formation. Glia. 2012; 60:1646–1659. [PubMed: 22782669]

Tajima M, Crane JM, Verkman AS. Aquaporin-4 (AQP4) associations and array dynamics probed by photobleaching and single-molecule analysis of green fluorescent protein-AQP4 chimeras. J Biol Chem. 2010; 285:8163–8170. [PubMed: 20071343]

Tradtrantip L, Zhang H, Saadoun S, Phuan PW, Lam C, Papadopoulos MC, Bennett JL, Verkman AS. Anti-aquaporin-4 monoclonal antibody blocker therapy for neuromyelitis optica. Ann Neurol. 2012; 71:314–322. [PubMed: 22271321]

Verbavatz JM, Ma T, Gobin R, Verkman AS. Absence of orthogonal arrays in kidney, brain and muscle from transgenic knockout mice lacking water channel aquaporin-4. J Cell Sci. 1997; 110:2855–2860. [PubMed: 9427293]

Wingerchuk DM, Lennon VA, Pittock SJ, Lucchinetti CF, Weinshenker BG. Revised diagnostic criteria for neuromyelitis optica. Neurology. 2006; 66:1485–1489. [PubMed: 16717206]

Yang B, Brown D, Verkman AS. The mercurial insensitive water channel (AQP-4) forms orthogonal arrays in stably transfected Chinese hamster ovary cells. J Biol Chem. 1996; 271:4577–4580. [PubMed: 8617713]

Yang B, van Hoek AN, Verkman AS. Very high single channel water permeability of aquaporin-4 in baculovirus-infected insect cells and liposomes reconstituted with purified aquaporin-4. Biochemistry. 1997; 36:7625–7632. [PubMed: 9200715]

Yang B, Zhang H, Verkman AS. Lack of aquaporin-4 water transport inhibition by antiepileptics and arylsulfonamides. Bioorg Med Chem. 2008; 16:7489–7493. [PubMed: 18572411]

Zhang H, Bennett JL, Verkman AS. Ex vivo spinal cord slice model of neuromyelitis optica reveals novel immunopathogenic mechanisms. Ann Neurol. 2011; 70:943–954. [PubMed: 22069219]

Zhang H, Verkman AS. Evidence against involvement of aquaporin-4 in cell-cell adhesion. J Mol Biol. 2008; 382:1136–1143. [PubMed: 18708067]

Zhang RB, Logee KA, Verkman AS. Expression of mRNA coding for kidney and red cell water channels in Xenopus oocytes. J Biol Chem. 1990; 265:15375–15378. [PubMed: 2394728]

Zeuthen T, Zeuthen E, Macaulay N. Water transport by GLUT2 expressed in Xenopus laevis oocytes. J Physiol. 2007; 579:345–361. [PubMed: 17158169]

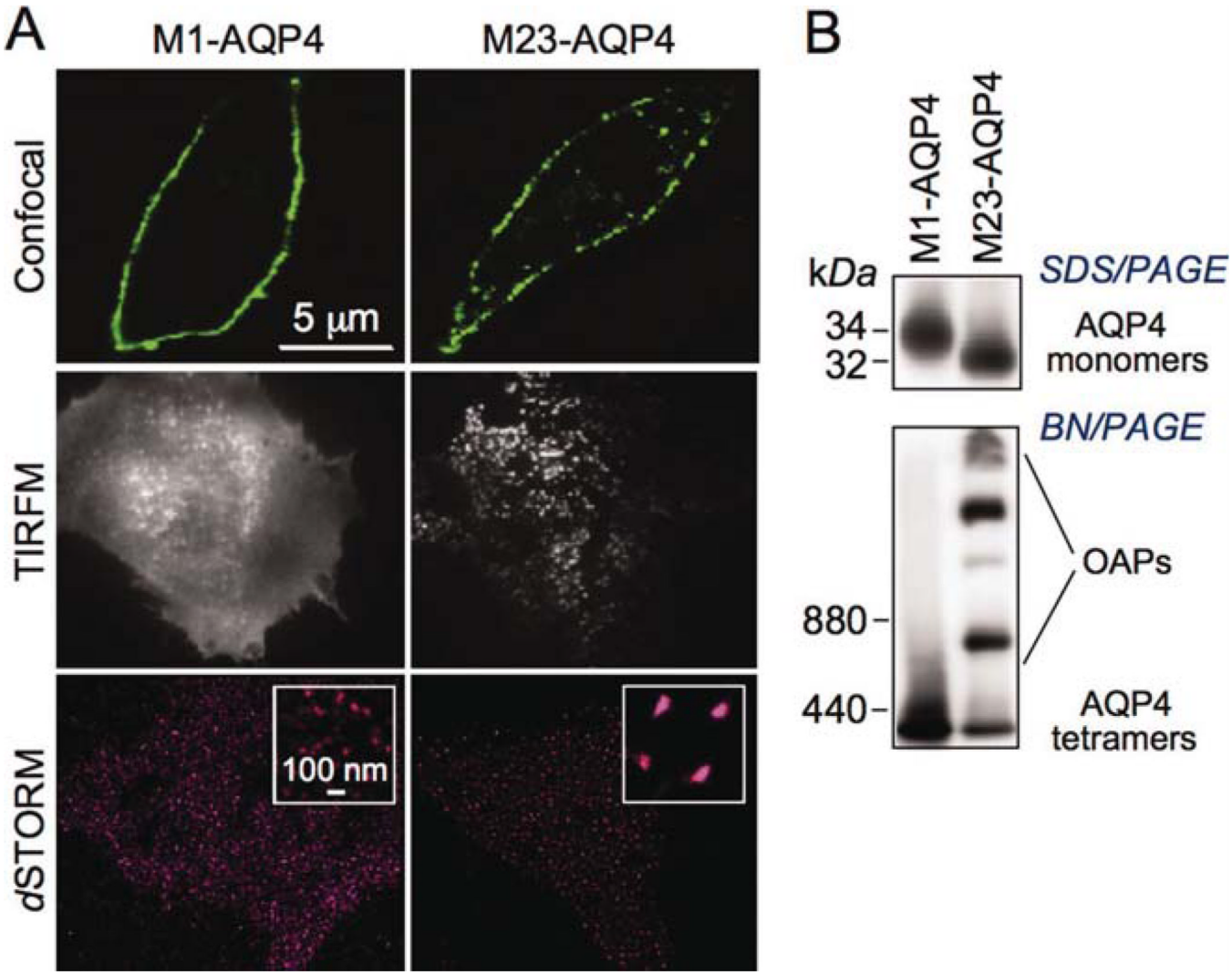

Fig. 1.

Characterization of AQP4-transfected CHO cells. (**A**) Immunofluorescence of CHO cells stably transfected with M1- or M23-AQP4, stained with anti-C-terminus AQP4 antibody and fluorescent secondary antibody, and imaged by confocal microscopy (top), TIRFM (middle), and *d*STORM (bottom). (**B**) AQP4 immunoblot of cell homogenate following SDS/PAGE (top) and (nondenaturing) BN/PAGE (bottom). [Color figure can be viewed in the online issue, which is available at wileyonlinelibrary.com.]

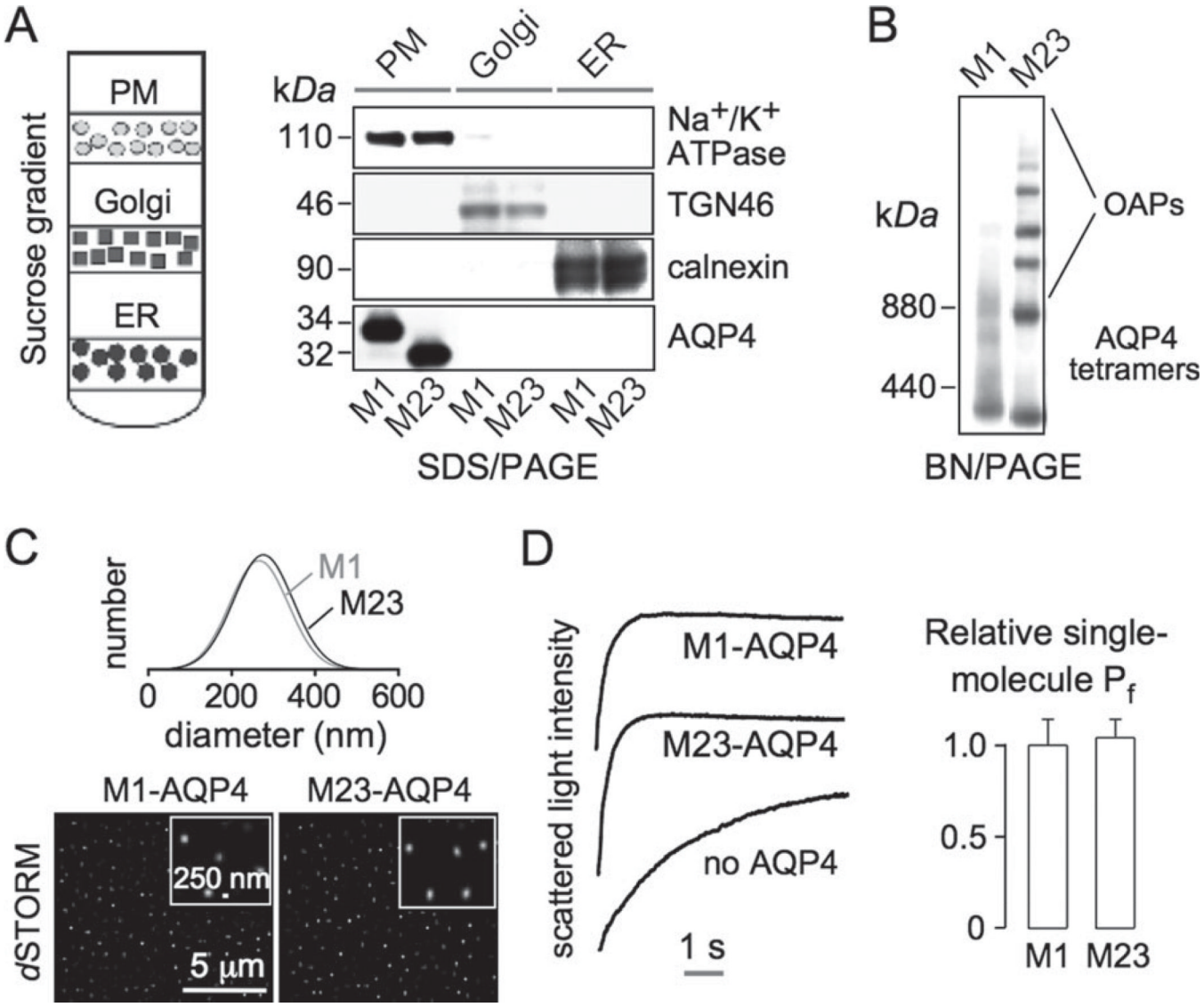

Fig. 2.

AQP4 supramolecular assembly in OAPs does not affect its single-molecule water permeability. (**A**) (left) Membrane fractionation method. (Right) Immunoblot of membrane fractions for AQP4 and indicated plasma membrane, Golgi, and ER markers. (**B**) AQP4 immunoblot following BN/PAGE of plasma membrane vesicles from M1- and M23-AQP4-transfected CHO cells. (**C**) Plasma membrane vesicle size determined by quasi-elastic light scattering (top) and by *d*STORM of surface-immobilized vesicles immunostained with AQP4 antibody. (**D**) Stopped-flow light scattering measurement of plasma membrane osmotic water permeability. (left) Plasma membrane vesicles from non-transfected and M1- or M23-AQP4-expressing cells were subjected to a 250-mM inwardly directed osmotic gradient, resulting in vesicle shrinkage (increased scattered light intensity). (Right) Relative single-molecule water permeability (P_f) deduced from light scattering, vesicle size, and AQP4 expression data (SE, $n = 5$, difference not significant).

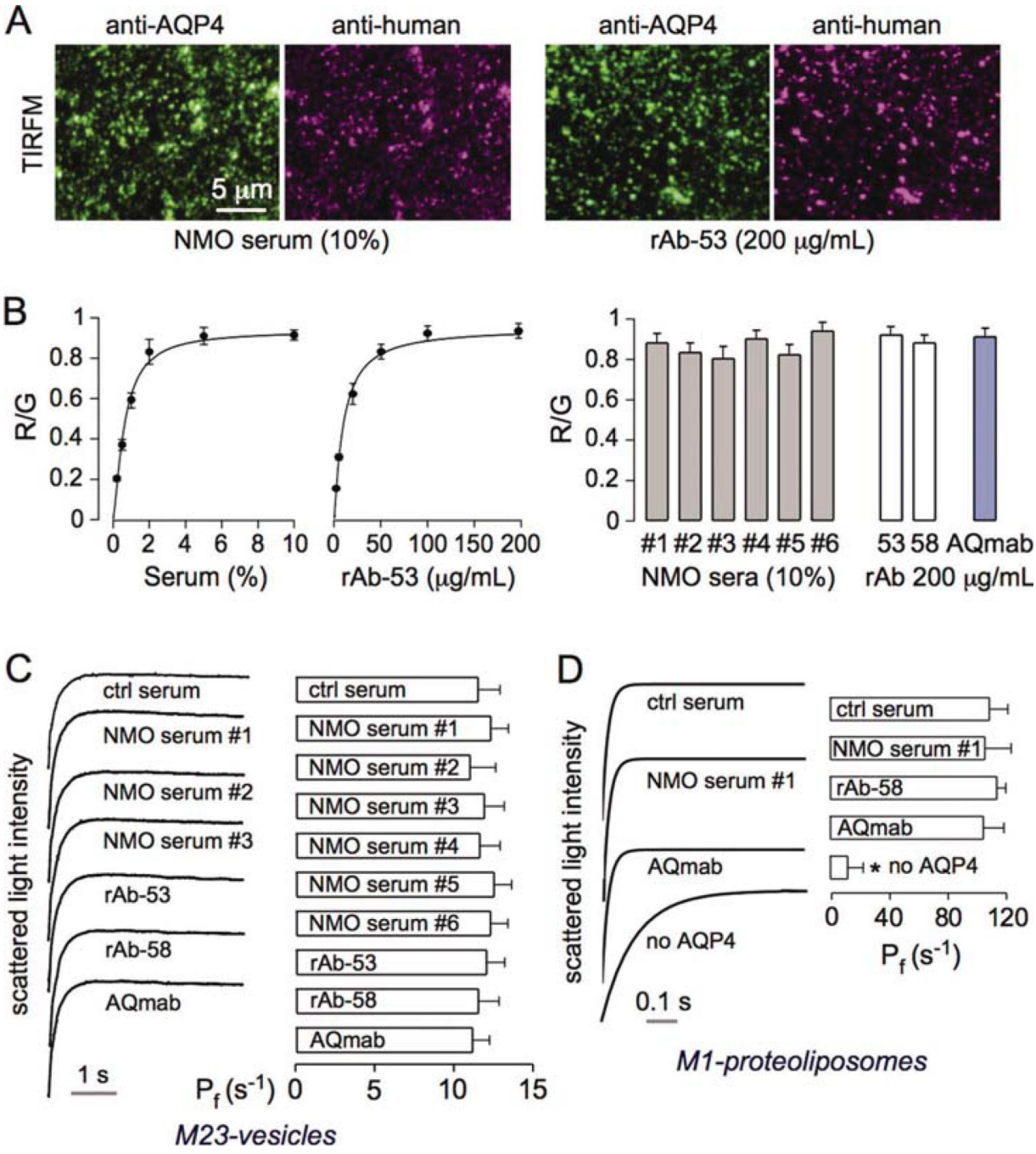

Fig. 3.

NMO-IgG does not inhibit AQP4 water permeability. (**A**) Plasma membrane vesicles from M23-AQP4-expressing CHO cells were immobilized on a coverglass, incubated with NMO serum (left) or recombinant NMO antibody (right), and immunostained green for AQP4 and red for NMO-IgG. (**B**) (left) Red-to-green fluorescence ratios for experiments as in A as a function of serum/rAb concentration (SEM, $n = 4$). Data fitted to saturable, single-site binding model. (Right) R/G for six different NMO sera and three rAbs. (**C**) Plasma membrane osmotic water permeability measured as in Fig. 2D. M23-AQP4-containing vesicles were incubated with sera/rAbs as in panel B. (Left) Representative light scattering

curves. (Right) Relative osmotic water permeability (P_f in s^{-1}) deduced from light scattering data (SE, $n = 5$, differences not significant). (**D**) Osmotic water permeability in control and AQP4-reconstituted proteoliposomes following NMO-IgG incubations as done in panel B (SE, $n = 5$, differences not significant). [Color figure can be viewed in the online issue, which is available at wileyonlinelibrary.com.]

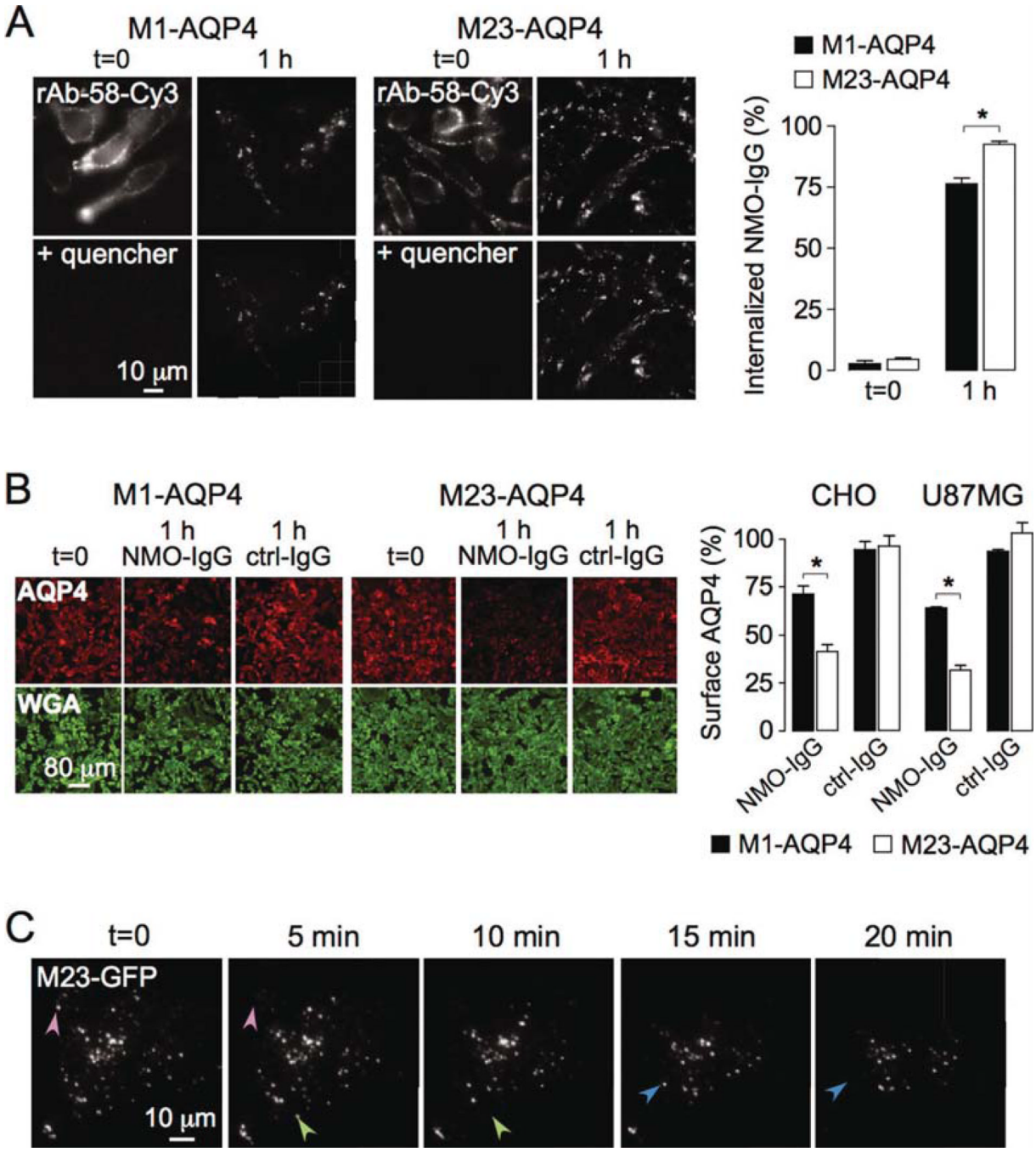

Fig. 4.

NMO-IgG binding causes greater internalization of M23-than M1-AQP4 when expressed separately in transfected cells. (**A**) CHO cells stably expressing M1- or M23-AQP4 were labeled with 20 μg/mL rAb-58-Cy3 at 4°C, washed, and chased for 1 h at 37°C. (Left) Cy3 fluorescence shown before ($t = 0$) and at 1 h chase. Fluorescence of rAb-58-Cy3 remaining at the cell surface was quenched with bromocresol green (+quencher). (Right) Percentage of internalized antibody after 0 and 1 h chase (SE, $n = 10$, $*P < 0.01$). Representative of two sets of experiments. (**B**) (Left) CHO cells expressing M1- or M23-AQP4 stained for surface AQP4 (red) and plasma membrane (WGA, green) before ($t = 0$) and after 1 h incubation at

37°C with 50 μg/mL NMO-IgG (rAb-58) or control-IgG (ctrl-IgG). (Right) Percentage of AQP4 remaining at the cell surface (SE, $n = 6$, $*P < 0.01$). Representative of two sets of experiments done on CHO and U87MG cells. (**C**) TIRFM of U87MG cells transfected with M23-AQP4/GFP chimera (M23-GFP), incubated with 50 μg/mL rAb58 for 1 h at 4°C, and then chased at 37°C for indicated times (full time course in Supp. Info. Movie 1). Arrowheads of the same color in consecutive micrographs show internalized OAPs. [Color figure can be viewed in the online issue, which is available at wileyonlinelibrary.com.]

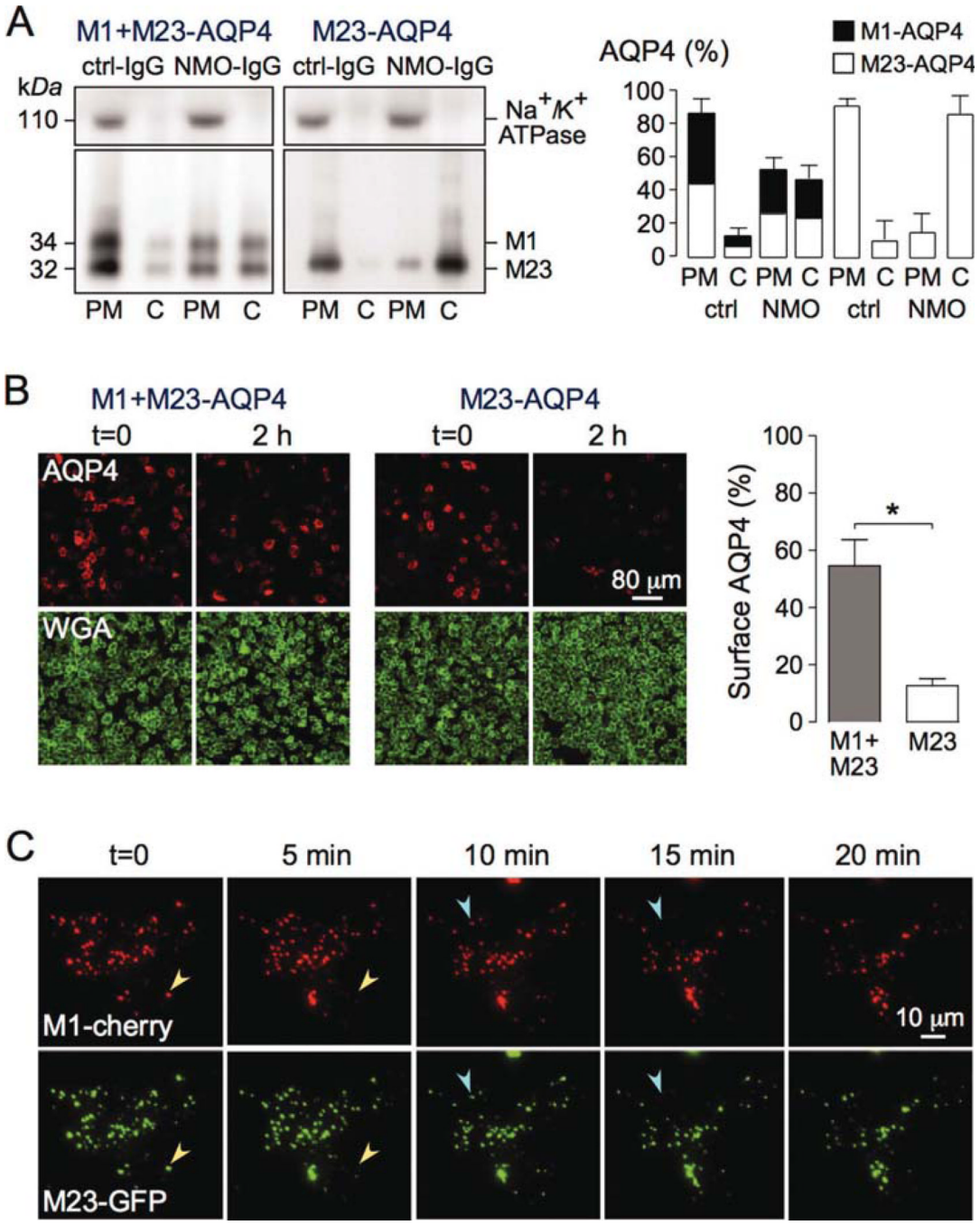

Fig. 5.

NMO-IgG binding causes simultaneous cointernalization of M1- and M23-AQP4 when coexpressed in transfected cells. (**A**) CHO cells were transiently transfected with M23-AQP4 only or together with an equal amount of M1-AQP4, and incubated with 50 μg/mL NMO-IgG (rAb-58) or control-IgG (ctrl-IgG) for 2 h at 37°C. (Left) Immunoblot of AQP4 and Na^+/K^+ ATPase following SDS/PAGE of plasma membrane (PM) and intracellular vesicles (cytoplasmic, C) fractions. (Right) M1- and M23-AQP4 amounts from blots as in A (SE, $n = 3$). (**B**) (Left) Cells treated as in A were stained for surface AQP4 (red) and plasma membrane (WGA, green). (Right) Percentage of remaining AQP4 at the cell surface after 2

h incubation with NMO-IgG (SE, $n = 10$, $*P < 0.01$). Representative of two sets of experiments. (**C**) TIRFM of U87MG cells transfected with M1-mCherry (red) and M23-GFP (green), incubated with 50 μg/mL rAb58 for 1 h at 4°C, and then chased at 37°C for indicated times (full time course in Supp. Info. Movie 2). Arrowheads of the same color in consecutive micrographs show internalized OAPs containing both isoforms. [Color figure can be viewed in the online issue, which is available at wileyonlinelibrary.com.]

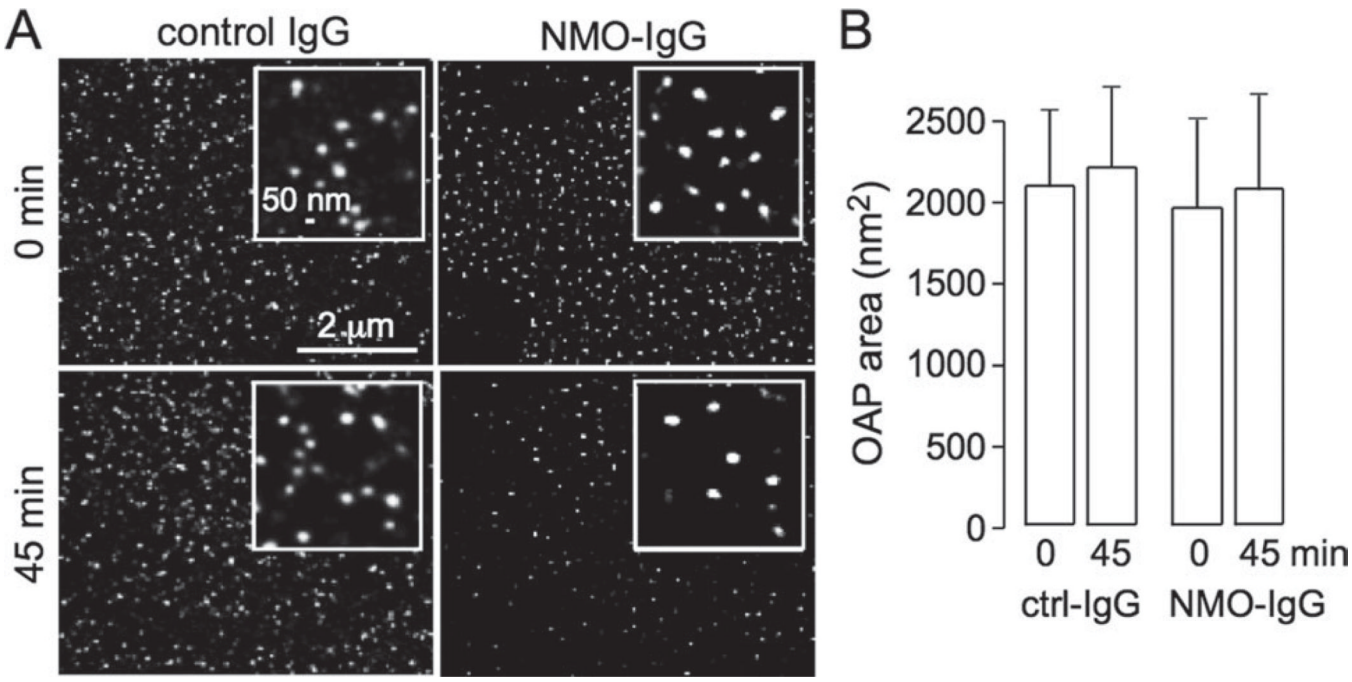

Fig. 6.

NMO-IgG does not cause cell surface AQP4 clustering. (**A**) Live cell PALM of cells cotransfected with M1- and M23-AQP4-PAmCherry. Cells imaged before (0 min) and at 45 min after incubation of NMO serum. (**B**) Average OAP area (SE, $n = 6$, difference not significant).

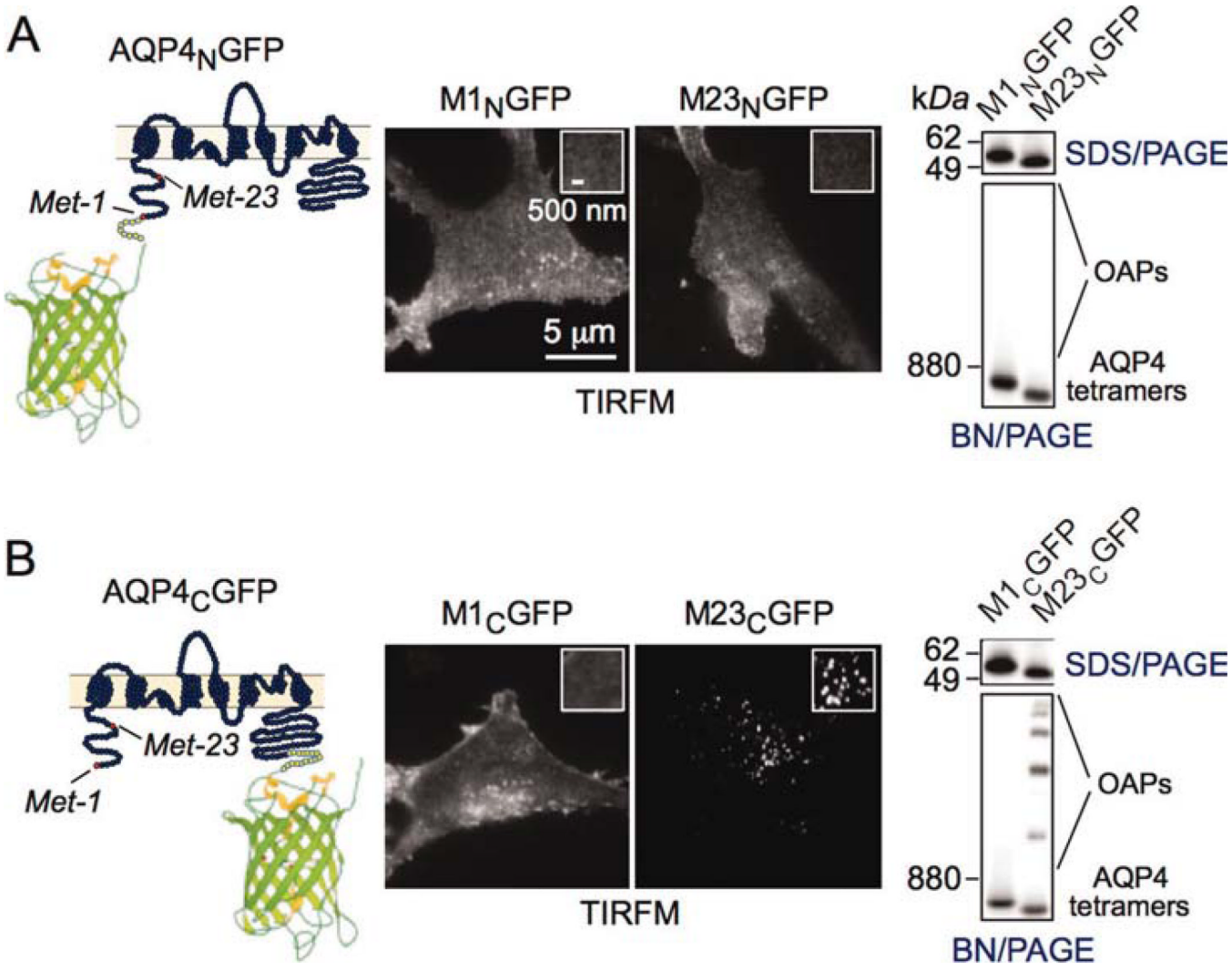

Fig. 7.

N-terminus GFP addition disrupts OAP formation by M23-AQP4. (**A**) N-terminus chimeras showing schematic (left), TIRFM (center), and BN/PAGE (right). (**B**) C-terminus chimera. [Color figure can be viewed in the online issue, which is available at wileyonlinelibrary.com.]